IEEE Access
Multidisciplinary | Rapid Review | Open Access Journal

Received November 21, 2019, accepted November 27, 2019, date of publication December 2, 2019,
date of current version December 12, 2019.

Digital Object Identifier 10.1109/ACCESS.2019.2956954

Development and Control of an MR Brake-Based Passive Force Feedback Data Glove

DAOMING WANG, YAKUN WANG, JIAWEI PANG, ZHENGYU WANG, (Member, IEEE), AND BIN ZI

School of Mechanical Engineering, Hefei University of Technology, Hefei 230009, China

Corresponding author: Zhengyu Wang (wangzhengyu_hfut@hfut.edu.cn)

This work was supported in part by the National Natural Science Foundation of China under Grant 91748109 and Grant 51805129, and in part by the Fundamental Research Funds for the Central Universities under Grant JZ2019HGTB0078.

ABSTRACT This paper presents the development and feedback force control of a safe, lightweight, yet powerful, and stable passive force feedback data glove (FFDG), utilizing a disc-type magnetorheological (MR) brake as the force feedback device. Firstly, a detailed illustration of the mechanical design of the FFDG, including transmission structure, MR brake, and angle measuring mechanism, is presented. Then, to achieve a precise feedback force control, the design and modelling of a current controller based on the buck circuit are carried out. This is followed by the tracking control of the feedback force, using conventional PID and adaptive fuzzy-PID control schemes. The control effect of the two methods is evaluated and compared through simulations. Finally, an experimental set-up is established, and a series of experiments are carried out on both the manufactured MR brake and the FFDG prototype. The results verify the feasibility and stability of the developed FFDG, and demonstrate that the feedback force tracking accuracy of the adaptive fuzzy-PID controller is satisfactory.

INDEX TERMS Force feedback data glove, magnetorheological brake, force feedback, current controller, adaptive fuzzy-PID control.

I. INTRODUCTION

With technological developments in aerospace, marine exploration, and atomic energy, there is an increasing need for robots that can work in environments that are too dangerous or unreachable for humans [1]. However, it is currently rather difficult to develop fully autonomous robots operating in unknown environments due to technological limitations of mechanisms, control systems, sensing systems, and artificial intelligence. Due to these reasons, master-slave teleoperation robots working in the human-robot interaction mode have attracted broad attention worldwide [2]–[4].

Force feedback data glove (FFDG) is an ideal interface device for human-machine-environment interactions. Hence, FFDG has been widely used in master-slave teleoperation systems. During the interaction between a slave robot and the environment, it is difficult to provide accurate control commands to the slave robot if the operator cannot feel the interaction force. In such situations, a precise feedback of the interaction force between the slave robot and the environment, to the operator's hand, through sensors and force feedback devices, can help the operator to provide more accurate control commands while adding his/her feelings to the master-slave operation system [5], [6]. Therefore, the immersive feelings experienced by the operator, by means of force telepresence technology, will greatly improve the operator's sense of telepresence. This enables the operator to manipulate the remote robot in order to accomplish various complex tasks more effectively and accurately [7].

There are generally two types of actuation mechanism, including active and passive type, for force feedback in the master-slave operation system [8]. Currently, the majority of active FFDGs adopt electric or pneumatic force feedback methods. Bouzit et al. [9] developed a pneumatic FFDG integrated with non-contact Hall-effect sensors to detect finger positions. The force feedback device is placed inside the palm to make the structure compact. Nakagawara *et al.* [10] proposed a motor-powered FFDG that can provide a feedback force to the operator's fingertips through motor drive and cable transmission. Ben-Tzvi *et al.* [11], [12] and Ma *et al.* [13] fabricated a haptic FFDG suitable for different operators. It utilizes five DC motors to provide a feedback

The associate editor coordinating the review of this manuscript and approving it for publication was Ludovico Minati.

This work is licensed under a Creative Commons Attribution 4.0 License. For more information, see http://creativecommons.org/licenses/by/4.0/

force and can track the hand movement through a linkage mechanism.

The passive FFDG is superior to the active FFDG in terms of safety and comfort. Conventional power brakes have the shortcoming of slow response, which may cause lack in quality of force feedback [8]. To address this problem, smart materials, such as shape memory alloys (SMAs), piezoelectric materials, electrorheological (ER) and magnetorheological (MR) materials, have been utilized as haptic generator for master-slave systems [8], [14]–[22]. The MR brake belong to MR fluids-based device, which can rapidly and reversibly change its resistance force in response to a magnetic field [23]. It also brings many attractive advantages including quiet and fast response with simple control, compact yet powerful and low energy consumption [24]. Winter *et al.* [25] developed an FFDG using a piston-type MR damper to provide feedback force. Compared to active resistance devices such as motors and pneumatic cylinders, the MR damper has a larger torque-to-weight ratio which makes it a better choice for the force feedback device [26]. Cassar *et al.* [27] proposed an FFDG which has two linear MR dampers for one finger. One damper is used to transmit feedback force to the Metacarpophalangeal (MCP) joint and the other to both the MCP and proximal interphalanx (PIP) joints. Qin *et al.* [28] developed a six degree-of-freedom (DOF) haptic hand controller equipped with three MR brakes to provide a maximum force of 8 N to the thumb, index, and middle fingers. The device is compact and powerful, and has a good dynamic performance. Okui *et al.* [29] designed a Delta-type 4-DOF force feedback device actuated with a MR clutch and pneumatic artificial muscles (PAMs).

To summarize, the active force feedback mode may cause damage to the operator if improperly operated [30]–[34]. Additionally, the motor used to produce sufficient feedback force is bulky and heavy. Hence, it is unsuitable to be placed on the operator's hand. Although there are a few works concerning the passive FFDG, the feedback force generated by a piston-type MR damper lacks stability because it is greatly affected by the grasping speed of the operator. Consequently, the major limitations that need to be fixed urgently in FFDGs are their safety and a lack of stability in the feedback force.

In view of this, the present study aims at developing a safe, lightweight, powerful, and stable passive FFDG. To accomplish this goal, a small-scale, disc-type MR brake is used as the force feedback device for each finger because its resistance force is less affected by the velocity [35], [36]. Furthermore, MR brakes are installed on the operator's arm to reduce the load and to avoid restricting the workspace of the hand. The feedback force generated by the MR brake is transmitted to the operator's fingertips though a lightweight and flexible Bowden-cable transmission mechanism. This configuration can alleviate the load on the hand in order to enhance the sense of telepresence. To further achieve an accurate telepresence force for the operator, a precise feedback force control is still necessary for the FFDG. According to the operating principle of the MR brake, the feedback force can be regulated solely by changing the coil current [37]. This paper presents the design and modelling of a buck circuit-based current controller, followed by the feedback force tracking control using both conventional proportional-integral-derivative (PID) and adaptive fuzzy-PID control schemes. The control effect is verified through simulations and experiments.

The rest of this paper is organized as follows: the mechanical design of the MR brake-based passive FFDG is illustrated in Section II. Section III presents the design and modelling of the current controller based on the buck circuit, as well as the feedback force tracking control of the designed FFDG. The experimental results are described in Section IV, and verify the feasibility and stability of the FFDG prototype. Finally, Section V presents the conclusions of this paper.

II. MECHANICAL DESIGN

In general, the design of an FFDG should satisfy the following criteria: (1) It is capable to provide a sufficient amount of feedback force; (2) It can accurately measure the finger angle during grasping; (3) It can help the operator experience a realistic sense of telepresence [38]–[41]. Based on the above principles, a novel passive FFDG, based on the disc-type MR brake, is designed as shown in Figure 1. It mainly consists of the transmission structure, force feedback device, angle measuring mechanism, exoskeleton, torsion spring, angle sensor, and cables. Five MR brakes are installed on the arm exoskeleton to avoid restricting the grasping space and reduce the load on the operator's hand. A flexible Bowden-cable transmission form is adopted in the transmission structure for long-distance transmissions of the feedback force. An indirect type angle measuring mechanism is also designed to measure the bending angle of the finger.

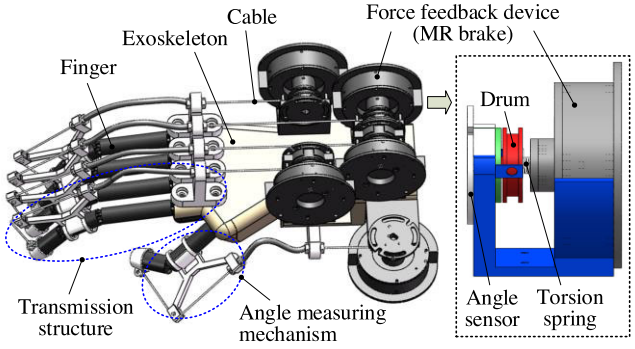

FIGURE 1. Configuration of the MR brake-based passive FFDG.

A. TRANSMISSION STRUCTURE

A Bowden-cable transmission structure is designed as shown in Figure 2. The structure includes a finger cot, a pulley, a support, and a set of Bowden-cables. The two ends of the Bowden are fixed with the support and angle measuring mechanism, respectively. The cable is connected to the finger cot through a Bowden and a pulley. While grasping, the feedback force is transmitted to the operator's fingertips to achieve the

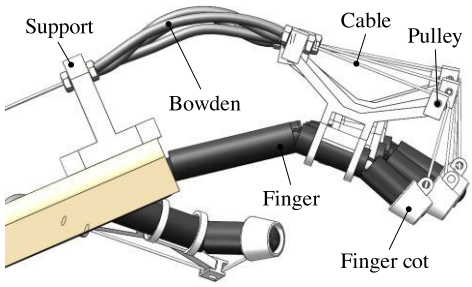

FIGURE 2. Schematic of the Bowden-cable transmission structure.

force feedback. A thin-film pressure sensor is adhesively attached to the fingertips to measure the actual feedback force on the fingertips, and to realize a closed-loop control of the feedback force.

B. FORCE FEEDBACK DEVICE

A disc-type MR brake shown in Figure 3 is designed as the force feedback device for the FFDG prototype. Main specifications of the MR brake are given in Table 1. It is composed of a shell, a shaft, an isolation ring, a disc, a coil, and several seal rings. The disc is connected to the shaft by screws and a circlip is used to adjust its axial position. The isolation ring, made of nonmagnetic material, is designed to reduce magnetic flux leakage. The working gap formed between the shell and the disc has a width of 1 mm and is filled with MR fluids. Several seal rings are utilized to prevent fluid leakage.

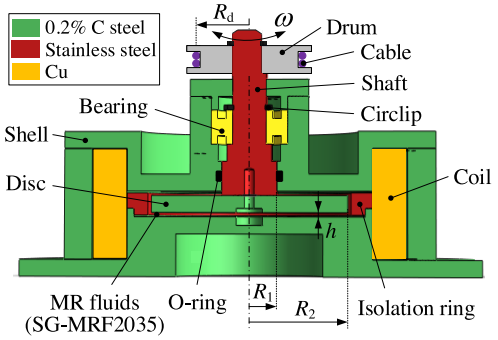

FIGURE 3. MR brake assembly.

TABLE 1. Main specifications of the MR brake.

Specification	Value
Outer diameter	54 (mm)
Total thickness	25 (mm)
Mass	190 (g)
Effective inner radius (R_1)	4 (mm)
Effective Outer radius (R_2)	14 (mm)
Gap thickness (h)	0.5 (mm)
No. of coil turns	180 (turns)
Copper wire for the coil	AWG 24

If the coil is not energized, the MR fluid exhibits a Newtonian state and the brake operates in a non-working state. At this time, a small torque is produced by the viscosity of the MR fluid. However, once the coil is energized, the MR fluid is converted to a solid-like state instantly [42], [43]. The total torque T is the sum of the field-induced torque T_B and viscous torque T_η [24], [44]

$$T = T_B + T_\eta = \frac{4}{3}\pi\tau_y(B)(R_2^3 - R_1^3) + \frac{\pi\eta\omega}{h}(R_2^4 - R_1^4) \quad (1)$$

where $\tau_y(B)$ is the field-induced shear stress of the MR fluid, which is a function of the magnetic induction B. η is the dynamic viscosity of the MR fluid, ω is the angular velocity of the shaft, R_1 and R_2 are the effective inner and outer radii of the working gap, respectively, and h is the gap thickness.

As shown in Figure 3, the shaft of the MR brake is connected to a drum through a flat key. Then, the relationship between the total torque T and the resistance force F of the MR brake is expressed as

$$T = F \cdot R_d \quad (2)$$

where R_d is the winding radius of cables on the drum, $R_d = 10$mm in this design.

To reduce the loss of magnetomotive force in non-working areas, it is necessary to effectively guide the magnetic flux lines and ensure that most of them pass through the working gap vertically. Two-dimensional magnetic circuit simulations of the MR brake are conducted using ANSYS®. In the simulations, the relative permeability of stainless steel is set to 1. The MR fluids and 0.2% C steel belong to nonlinear ferromagnetic materials, whose magnetic properties are defined by the B–H curves shown in Figure 4.

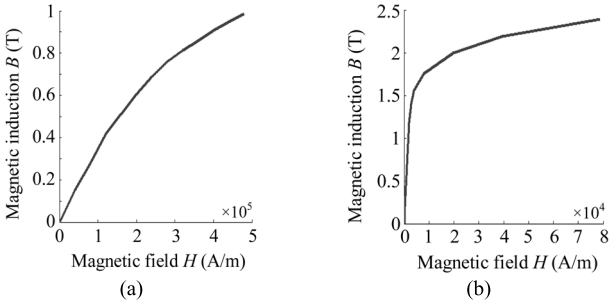

FIGURE 4. B–H curves of the nonlinear ferromagnetic materials: (a) MR fluids; (b) 0.2% C steel.

The results of the magnetic circuit simulations are depicted in Figure 5. In Figure 5(a) and 5(b), the current is set as 1 A. It is seen that the magnetic flux lines are strictly limited in the designed circuit as expected. This verifies the rationality and correctness of the circuit design and material selection. As observed in Figure 5(c), the magnetic induction is distributed evenly in the working gap with an average value of about 0.29 T at 1 A. Combining with the material parameters of the MR fluid and the dimensions of the MR brake, the maximum total torque is calculated as 0.21 N·m. Thus, the

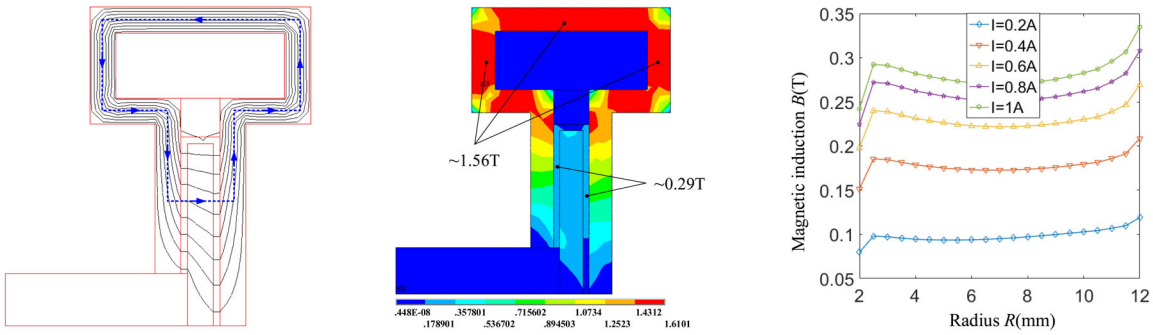

FIGURE 5. Results of the magnetic circuit simulations: (a) magnetic flux distribution; (b) magnetic induction contour; (c) magnetic induction distribution in the radial direction of the working gap.

maximum resistance force is 21 N, which is larger than the expected value of 20 N. Therefore, it is concluded that the MR brake satisfies the design requirements.

C. ANGLE MEASURING MECHANISM

Generally, traditional data gloves measure the bending angle of the finger joint directly through the use of bending sensors. The limitations of this approach include: 1) the deformation at any position of the hand will be mistakenly recognized as the bending of finger joints; 2) insufficient contact of the hand with the exoskeleton may produce slippage that decreases the measuring accuracy.

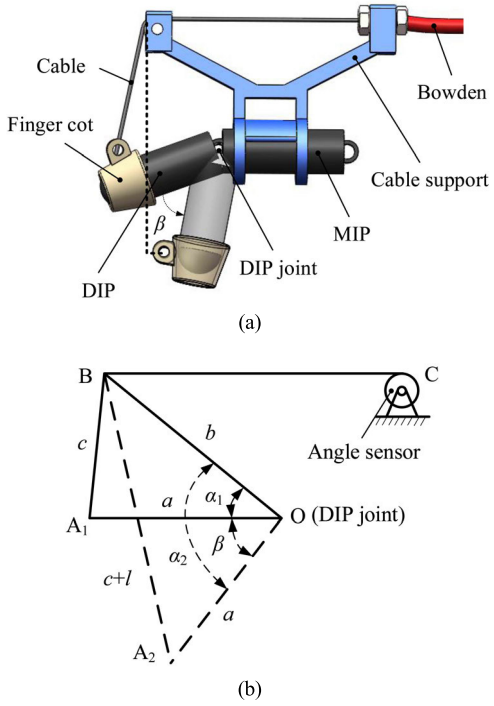

FIGURE 6. Measuring principle of the bending angle for finger joints: (a) measuring mechanism; (b) geometric relationship.

Since the size of the angle sensor is relatively larger than the size of the finger, it may restrict the finger motion if directly installed on the fingertips of the operator. Thus, an indirect measuring method, shown in Figure 6, is adopted to detect the joint angle. A cable support is fixed on the middle phalanx (MP). While grasping, as the distal phalanx (DP) rotates over a certain angle, the length of the cable is elongated correspondingly. The elongation value of the cable length can be calculated based on the drum radius and the angle measured by the angle sensor. The rotation angle of DP is then determined using the law of Cosines. The triangle composed of the DP, cable, and cable support is equivalent to OA1B and OA2B, as presented in Figure 6(b). The lengths of OA1 and OA2 are both a and that of OB is b. The original cable length, when the finger is straight, is c. It changes to $c + l$ as the finger rotates over an angle β. According to the geometrical relationship shown in Figure 6(b), the bending angle of the DP is deduced as

$$\beta = \arccos\left[\frac{a^2 + b^2 - (c+l)^2}{2ab}\right] - \arccos\left(\frac{a^2+b^2-c^2}{2ab}\right) \quad (3)$$

Referring to the literature [33], the bending angles of the proximal phalanx (PP), MP, and DP approximately follow a coupling relationship of 1:1.5:1 while grasping. After measuring the bending angle of the DP, the bending angles of the other two phalanxes can be obtained by the above-mentioned coupling relationship.

III. FEEDBACK FORCE CONTROL

As mentioned above, a precise feedback force control is critical for the FFDG to provide an accurate sense of telepresence to the operator. The MR brake produces a feedback force when it is excited by the current. Therefore, to obtain a rapidly and controllable varying current, it is necessary to develop a high-speed current controller [45], [46]. In this study, a current controller based on the buck circuit is proposed, and its operating principle is shown in Figure 7. The primary circuit topology consists of a power metal-oxide-semiconductor field effect transistor (MOSFET) Q, a filter inductance L, a filter capacitor C, a diode D, a coil resistance R_M, and a coil inductance L_M. The input and output voltages of the circuit are denoted as U_i and U_o, respectively. As shown in Figure 8, by controlling the ON and OFF states of the MOSFET, the working states of the circuit can be altered to generate varying amounts of current.

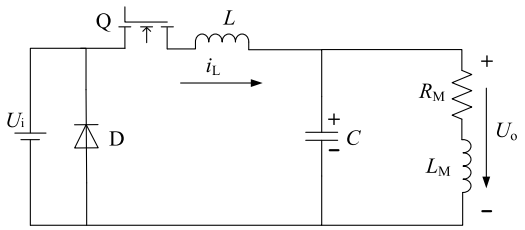

FIGURE 7. Schematic diagram of the buck circuit.

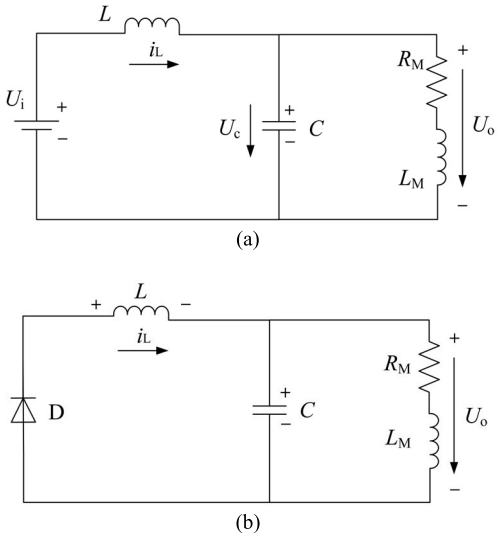

FIGURE 8. Working states of the buck circuit: (a) ON-state; (b) OFF-state.

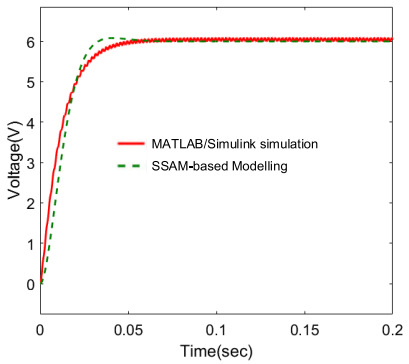

FIGURE 9. Comparison of response curves obtained by MATLAB/Simulink simulation and SSAM-based modelling.

Based on Kirchhoff's laws, the differential equation of the circuit in the ON-state is written as

$$\begin{cases} L\dfrac{\mathrm{d}i_\mathrm{L}}{\mathrm{d}t} = U_\mathrm{i} - U_\mathrm{c} \\ C\dfrac{\mathrm{d}U_\mathrm{c}}{\mathrm{d}t} = i_\mathrm{L} - i_{L_\mathrm{M}} \\ U_\mathrm{c} = R_\mathrm{M} i_{L_\mathrm{M}} + L_\mathrm{M}\dfrac{\mathrm{d}i_{L_\mathrm{M}}}{\mathrm{d}t} \end{cases} \tag{4}$$

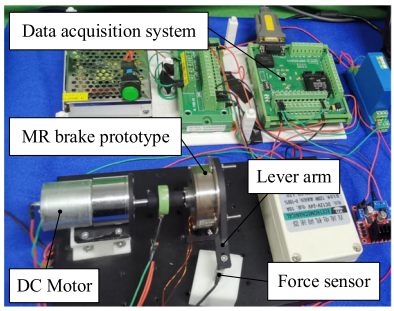

FIGURE 10. Test rig for measuring the force characteristic of the MR brake.

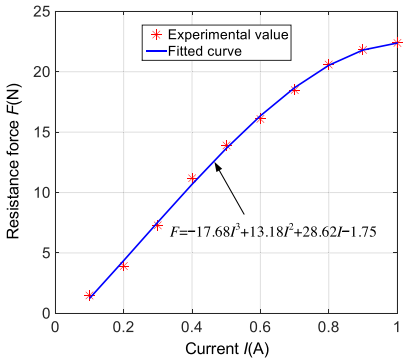

FIGURE 11. Resistance force versus current for the MR brake.

Similarly, the differential equation of the circuit in the OFF-state is given by

$$\begin{cases} L\dfrac{\mathrm{d}i_\mathrm{L}}{\mathrm{d}t} + U_\mathrm{c} = 0 \\ C\dfrac{\mathrm{d}U_\mathrm{c}}{\mathrm{d}t} = i_\mathrm{L} - i_{L_\mathrm{M}} \\ U_\mathrm{c} = R_\mathrm{M} i_{L_\mathrm{M}} + L_\mathrm{M}\dfrac{\mathrm{d}i_{L_\mathrm{M}}}{\mathrm{d}t} \end{cases} \tag{5}$$

where i_L and i_{L_M} are the currents of the filter inductance L and coil inductance L_M, respectively, and U_c is the voltage across the filter capacitor C.

In this study, i_L, U_c, and i_{L_M} are selected as the state variables of the circuit. Then, the equations of the ON and OFF states of the ideal buck circuit in each operation cycle are separately derived as

$$\begin{bmatrix} \dfrac{\mathrm{d}i_\mathrm{L}}{\mathrm{d}t} \\ \dfrac{\mathrm{d}i_{L_\mathrm{M}}}{\mathrm{d}t} \\ \dfrac{\mathrm{d}U_\mathrm{c}}{\mathrm{d}t} \end{bmatrix} = \begin{bmatrix} 0 & 0 & -\dfrac{1}{L} \\ 0 & -\dfrac{R_\mathrm{M}}{L_\mathrm{M}} & \dfrac{1}{L_\mathrm{M}} \\ \dfrac{1}{C} & -\dfrac{1}{C} & 0 \end{bmatrix} \begin{bmatrix} i_\mathrm{L} \\ i_{L_\mathrm{M}} \\ U_\mathrm{c} \end{bmatrix} + \begin{bmatrix} \dfrac{1}{L} \\ 0 \\ 0 \end{bmatrix} U_\mathrm{i} \tag{6}$$

$$\begin{bmatrix} \dfrac{\mathrm{d}i_\mathrm{L}}{\mathrm{d}t} \\ \dfrac{\mathrm{d}i_{L_\mathrm{M}}}{\mathrm{d}t} \\ \dfrac{\mathrm{d}U_\mathrm{c}}{\mathrm{d}t} \end{bmatrix} = \begin{bmatrix} 0 & 0 & -\dfrac{1}{L} \\ 0 & -\dfrac{R_\mathrm{M}}{L_\mathrm{M}} & \dfrac{1}{L_\mathrm{M}} \\ \dfrac{1}{C} & -\dfrac{1}{C} & 0 \end{bmatrix} \begin{bmatrix} i_\mathrm{L} \\ i_{L_\mathrm{M}} \\ U_\mathrm{c} \end{bmatrix} + \begin{bmatrix} 0 \\ 0 \\ 0 \end{bmatrix} U_\mathrm{i} \tag{7}$$

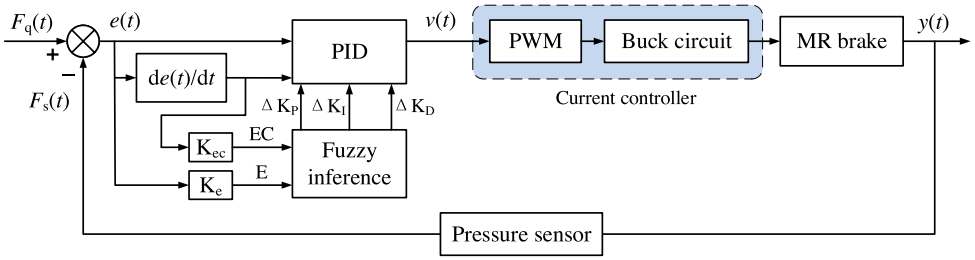

FIGURE 12. Block diagram of the adaptive fuzzy-PID-based feedback force controller.

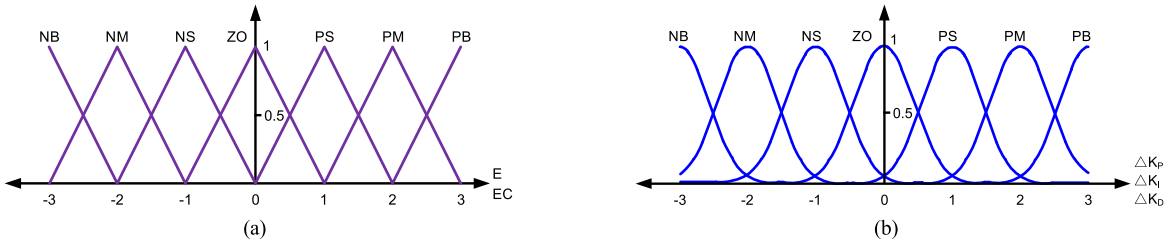

FIGURE 13. Membership functions for (a) E, EC; (b) K_P, K_I, K_D.

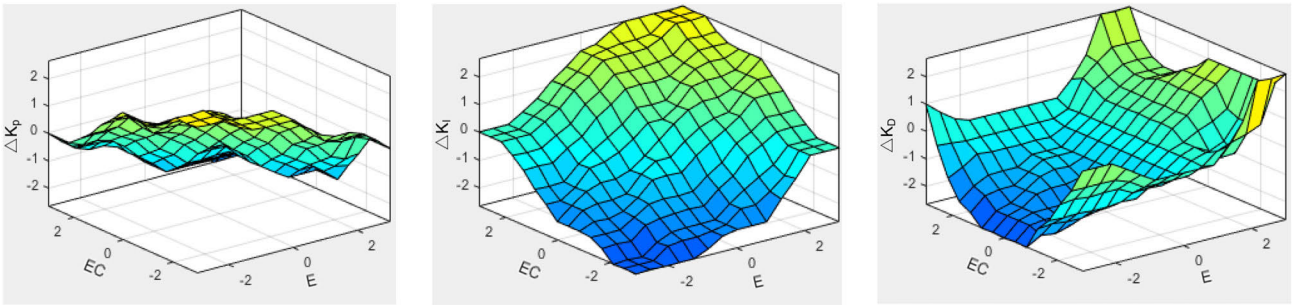

FIGURE 14. Output surface diagram of the fuzzy interface.

By averaging Eqs. (6) and (7) using the state-space averaging method (SSAM), the average state equation is calculated as

$$\begin{bmatrix} \frac{di_L}{dt} \\ \frac{di_{L_M}}{dt} \\ \frac{dU_c}{dt} \end{bmatrix} = \begin{bmatrix} 0 & 0 & -\frac{1}{L} \\ 0 & -\frac{R_M}{L_M} & \frac{1}{L_M} \\ \frac{1}{C} & -\frac{1}{C} & 0 \end{bmatrix} \begin{bmatrix} i_L \\ i_{L_M} \\ U_c \end{bmatrix} + \begin{bmatrix} \frac{d_R}{L} \\ 0 \\ 0 \end{bmatrix} U_i \quad (8)$$

where d_R is the duty ratio of the MOSFET, $d_R = \frac{t_{on}}{T_s}$, t_{on} denotes the switch-on time, and T_s the switching period.

Then, the transfer function of the circuit from duty ratio to output voltage is

$$\frac{\hat{U}_o(s)}{\hat{d}_R(s)}_{\hat{U}_i(s)=0} = \frac{U_i}{\frac{Ls}{R_M+L_Ms} + LCs^2 + 1} \quad (9)$$

By considering the filter capacitor and filter inductor as ideal circuit elements, the parameters of the buck circuit are listed as $U_i = 12$ V, $L = 150$ mH, $C = 400$ μF, $R_M = 12$ Ω, and $L_M = 1$ μH. Substituting the above parameters in Eq. (9),

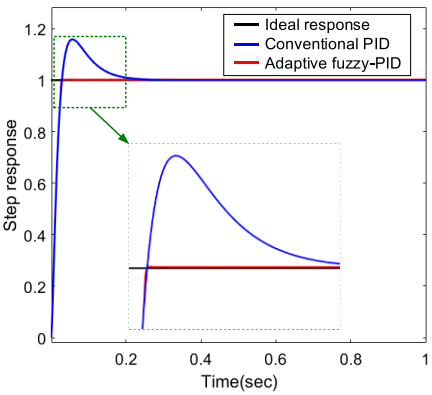

FIGURE 15. Unit-step responses of the feedback force for the conventional PID and adaptive fuzzy-PID controllers.

the transfer function is written as

$$\frac{\hat{U}_o(s)}{\hat{d}_R(s)}_{\hat{U}_i(s)=0} = \frac{144+12\times10^{-6}s}{6\times10^{-11}s^3+72\times10^{-5}s^2+0.150001s+12} \quad (10)$$

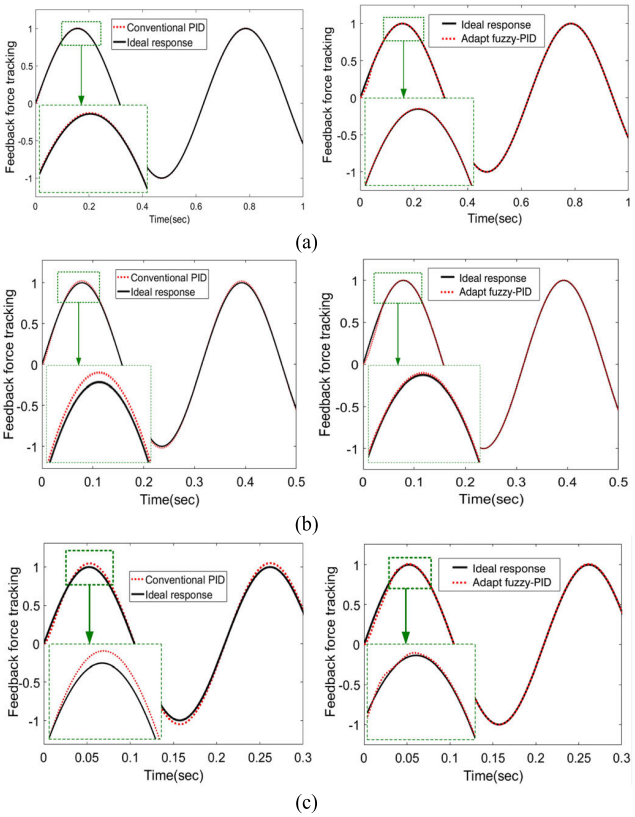

FIGURE 16. Sinusoidal responses of the feedback force at three different frequencies: (a) 10 Hz; (b) 20 Hz; (c) 30 Hz.

To evaluate the validity of the SSAM-based modelling method, a MATLAB/Simulink simulation of the ideal buck circuit is conducted, and the response curve is compared with the curve obtained from the modeling, as shown in Figure 9. A certain deviation is found between the two methods at the early stage of response. It is possible that this deviation is induced because the high-frequency variation of the switching period was neglected during modeling. Nonetheless, it should be noted that the two response curves are basically identical at the steady state. The phenomenon indicates that the SSAM-based modeling method can generally reflect the response of the buck circuit, thus proving its effectiveness and feasibility.

In the control system of the FFDG, the feedback force is regulated by changing the current. The transfer function of an MR brake is given by [47]

$$G(s) = \frac{F(s)}{I(s)} = \frac{K_0}{T_0 s + 1} \mathrm{e}^{-\tau s} \tag{11}$$

where $I(s)$ is the current, $F(s)$ is the resistance force, τ is the time lag constant, T_0 is the time constant, and K_0 is the gain.

Because τ is an extremely small value, $\mathrm{e}^{-\tau s}$ can be considered as $\frac{1}{1+\tau s}$. Then, the transfer function of the MR brake is

$$G(s) = \frac{F(s)}{I(s)} = \frac{K_0}{(T_0 s + 1)(1 + \tau s)} \tag{12}$$

The relationship between the resistance force and current of the MR brake is measured using a test rig with a DC motor, a lever arm, a force sensor, an MR brake prototype, and a data acquisition system (see Figure 10). The results are obtained as shown in Figure 11.

The experimental results of the resistance force and current are employed as the input and output data, respectively, for parameter identification using an identification toolbox in MATLAB. Then, the specific form of the transfer function for the designed MR brake is obtained as

$$G(s) = \frac{-1.2455 \times 10^7}{(4746.4s + 1)\,(1 + 0.3737s)} \tag{13}$$

As generic feedback controllers, both the conventional PID and adaptive fuzzy-PID controllers have been widely applied to several applications [48]–[52]. In this study, the two control schemes are adopted for the feedback force control of the FFDG. The control gains are determined by trial and error method based on the designer's experiences. Figure 12 exhibits the block diagram of the adaptive fuzzy-PID-based feedback force controller. As observed, the desired feedback force $F_q(t)$ is used as the control input and the actual feedback force $F_s(t)$ detected by a pressure sensor as the control output. The deviation $e(t)$ and its variation $ec(t)$ are considered as the input parameters for the fuzzy interface. After defuzzification, the PID parameters are adjusted in order to control the change in the feedback force.

Figure 13 displays the selection of membership functions for the input and output variables. The triangular type membership function is selected for the input variables E, EC, while the Gauss type membership function for the output variables ΔK_P, ΔK_I, ΔK_D. The output surface diagram of the fuzzy interface is shown in Figure 14.

Figure 15 presents the unit-step responses of the feedback force for the conventional PID and adaptive fuzzy-PID controllers. It is seen that the feedback force controlled by the adaptive fuzzy-PID can quickly reach stability while possessing a good control effect. To further evaluate the tracking performance of the feedback force, the sinusoidal responses of the feedback force at three different frequencies are simulated as shown in Figure 16. For a sinusoidal signal of 10 Hz, both the two controllers exhibit a good tracking effect. However, as the frequency increases to 20 Hz, a small tracking error is observed in the conventional PID controller. Furthermore, the tracking error in the conventional PID becomes larger once the frequency increases to 30 Hz while the adaptive fuzzy-PID controller maintains a good tracking performance. Therefore, it can be concluded that the adaptive fuzzy-PID controller is more suitable for the feedback force control of the MR brake-based FFDG.

IV. EXPERIMENTS

An experimental set-up is established to evaluate the performance of the FFDG prototype. As shown in Figure 17, the set-up consists of a computer, a data acquisition card (DAQ), the FFDG prototype, a current controller, and a

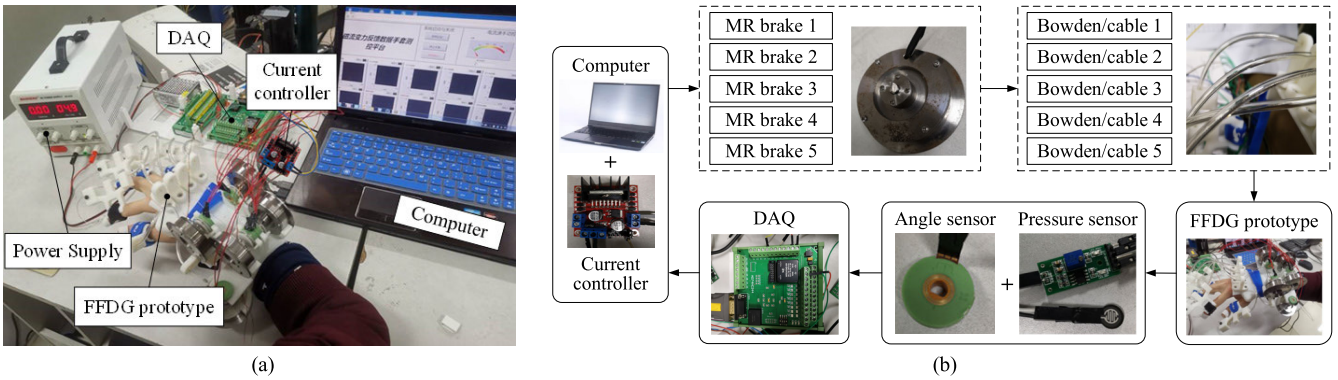

FIGURE 17. Experimental set-up. (a) experimental prototype. (b) system composition block diagram.

power supply. A detailed description of main apparatuses in the set-up is listed in Table 2. During the experiments, the current controller provides a variable current for the MR brake to generate a controllable resistance force. The resistance force is transmitted to the fingertips of the operator through cables. Simultaneously, the feedback force and the bending angle are measured by the pressure sensor and angle sensor, respectively. The measure data are then converted by the DAQ and transmitted to the computer for processing and analysis. Because the biological properties of the other four fingers, except the thumb, are similar, the following experiments are conducted by considering the middle finger of the operator as an example.

A. MR BRAKE EXPERIMENTS

The force output and time response characteristics of the MR brake greatly influence the stability and accuracy of the feedback force for the FFDG, which are measured using the test rig in Figure 10.

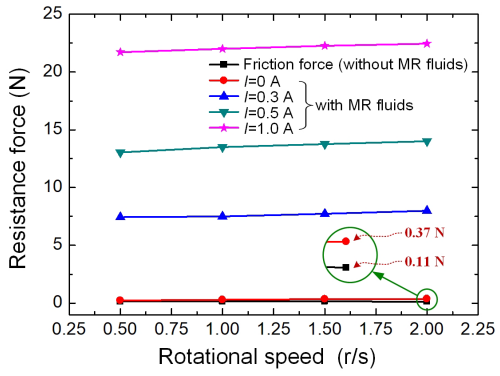

FIGURE 18. Resistance force versus rotational speed at different currents.

Five repeated experimental trials are carried out to measure the resistance force under various conditions. In each trial, the rotational speed ranges from 0.5 r/s to 2 r/s in increments of 0.5 r/s. Figure 18 shows the resistance force versus rotational speed at different currents. Without MR fluids in the working gap, the friction force, generated by the frictions of bearings and rotary rings, is found to be very small. For a speed of 2 r/s, the value of friction force is only 0.11 N, which is negligible compared with the field-induced force. Moreover, it is observed that the effect of speed is minimal on the resistance force. At 1 A, as the speed increase from 0.5 r/s to 2 r/s, the resistance force presents a slight increase from 21.42 N to 22.46 N with an increasing ratio of nearly 4.85%.

The time response of an MR fluids-based system includes the rheological response of MR fluids, the electromagnetic response of magnetic circuit, and the time lag of current controller. Several experiments are conducted to evaluate the force response of the MR brake. In the experiments, the motor rotates at a speed of 1 r/s and a current is applied to the MR brake at 15 ms and cut off at 75 ms.

As presented in Figure 19(a), the response time increase with the current. Its value varies between 15 ms and 30 ms as the current increases from 0.3 A to 1 A. In addition, a time lag is found in the current controller with a value of about 20 ms, which accounts for the majority of the total response time, about 66.7% at 1 A. Furthermore, the effect of particle sedimentation on the response of the MR brake is tested as depicted in Figure 19(b). It is visible that there is a slight time delay (less than 3 ms) on the response of the MR brake after placed for a few days. The phenomenon mainly occurs at the beginning of the force response. However, the effect of sedimentation can be eliminated by performing several repeated grasping actions before use.

In conclusion, even though there exists a certain amount of time delay on both the MR brake and current controller, the values are very small compared with the grasping period of a human hand, which usually takes about a few seconds. Therefore, the developed MR brake and the buck circuit-based current controller satisfy the response requirements for application in the FFDG.

B. ANGLE MEARURING EXPERIMENTS

Three repeated grasping experiments are carried out and the variation curves of the bending angle of the DP are recorded as shown in Figure 20. The bending angle increases steadily during grasping. This indicates that the angle measuring

TABLE 2. A detailed description of main apparatuses in the set-up.

Apparatus	Model	Manufacturer	Performance parameters
Data acquisition card (DAQ)	USB-6009	National Instruments	Sampling rate: 48 kS/s
Angel sensor	R24HS	Shenzhen MINOR Electronics Co., Ltd	Angle range: 345°±5°; Precision: 0.3%
Pressure sensor	FSR402	Interlink Electronics Co., Ltd	Force range: 0–20 N·m
Power supply	MT152D	Shanghai Maisheng Industrial Co., Ltd	Output voltage: 0–15 V

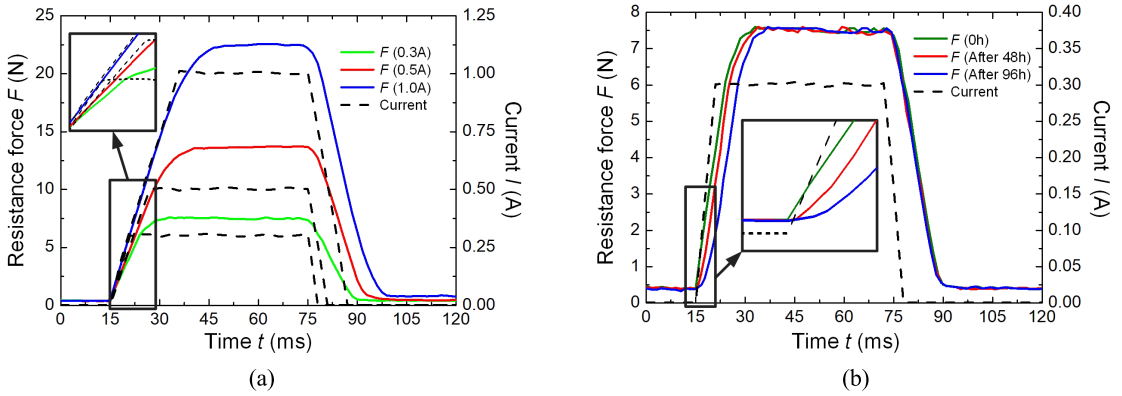

FIGURE 19. Resistance force responses of the MR brake. (a) at different currents; (b) the effect of particle sedimentation.

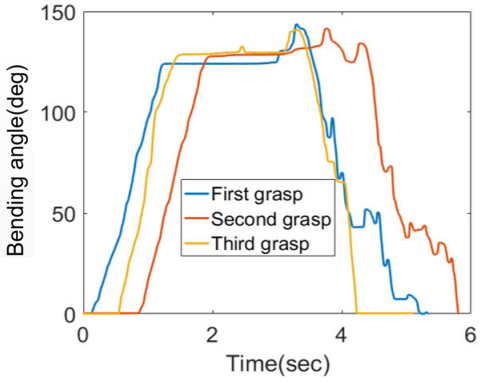

FIGURE 20. Variation curves of the bending angle of the DP.

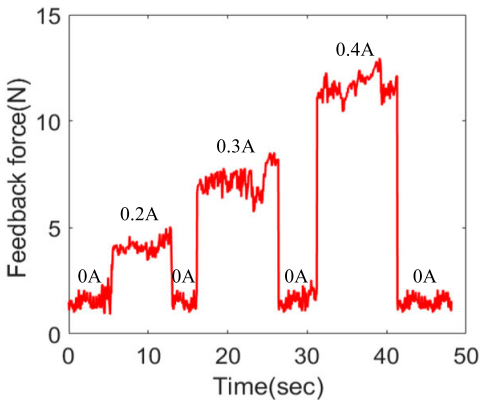

FIGURE 21. Feedback force on the fingertip for different currents during several grasping actions.

mechanism has good stability. In addition, the average ultimate bending angle of the DP is 133.8°. This value coincides with the actual ultimate angle of the DP of the operator which is measured to be 135°. A slight deviation is still found due to the inevitable restriction caused by the FFDG, in finger grasping. Overall, the experimental results prove the rationality and accuracy of the designed indirect-type angle measuring mechanism.

C. FEEDBACK FORCE STABILITY EXPERIMENTS

Figure 21 exhibits the variations in the feedback force on the fingertips during several grasping actions. Without applying a current to the MR brake, the feedback force on the fingertip is nearly 1 N. This feedback force mainly includes the viscous resistance force of the MR brake and the friction of the Bowden-cable transmission mechanism. For different currents of 0.2 A, 0.3 A, and 0.4 A, the average values of the feedback force are 4.1 N, 7.6 N, and 11.6 N, respectively. The values of the feedback force are generally steady during the entire grasping process. This agrees with the test results for the MR brake in Figure 11. This phenomenon verifies the stability and accuracy of the transmission mechanism and the resistance device. At a current of 0.4 A, the feedback forces for both slow and quick grasping actions are measured as shown in Figure 22. It is found that the grasping speed has little influence on the feedback force, thus demonstrating the feasibility and stability of the disc-type MR brake which was used as the force feedback device. Nevertheless, an unwanted chattering in found in the feedback force. It is mainly induced

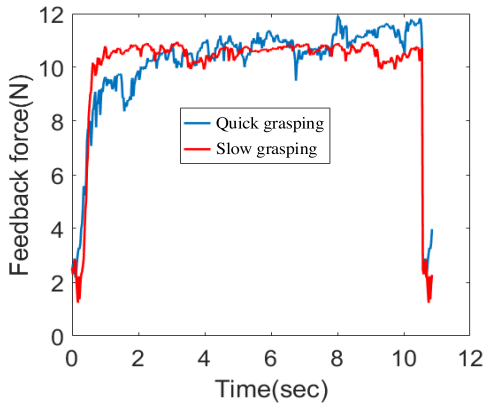

FIGURE 22. Influence of grasping speed on the feedback force.

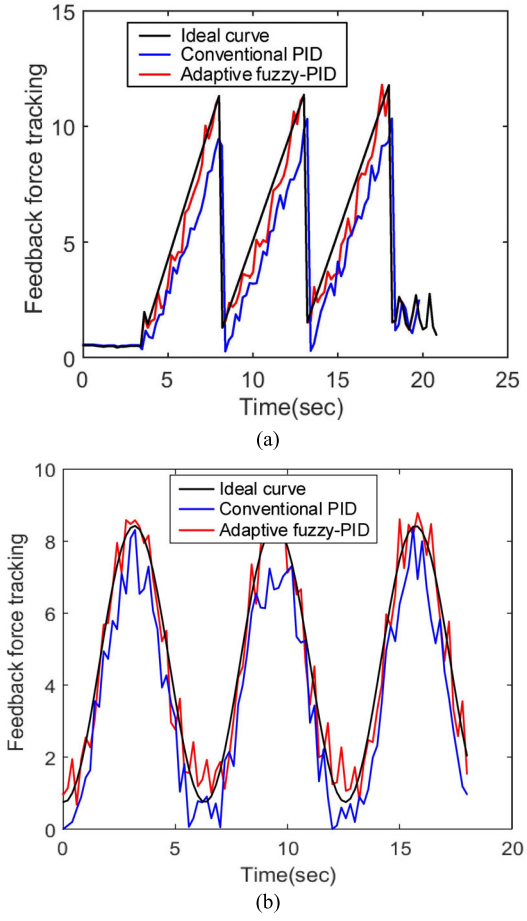

FIGURE 23. Feedback force tracking results using both conventional PID and adaptive fuzzy-PID controllers: (a) ramp signal; (b) sinusoidal signal.

by the jitter of fingers while overcoming the resistance force of MR brake, which causes the reduction in the measuring accuracy of the thin-film pressure sensor adhesively attached to the fingertips.

D. FEEDBACK FORCE TRACKING CONTROL EXPERIMENTS

Both conventional PID and adaptive fuzzy-PID controllers are used in the feedback force tracking control experiments. Figure 23 presents the feedback force tracking results in cases of both ramp and sinusoidal signals. During the experiments, a continuously changing current is applied to the MR brake by the current controller, based on the ideal value and the deviation of the feedback force. As observed, the adaptive fuzzy-PID is superior to the conventional PID in quality of tracking control. During the increasing stage, the actual feedback force can be quickly and precisely adjusted to follow the ideal curve. By contrast, the feedback force unloads immediately once the current cuts off. This phenomenon indicates that the adaptive fuzzy-PID has a relatively good tracking accuracy. However, there is still a slight tracking error, which is mainly caused by a certain amount of time lag in the current controller, the measuring error of the thin-film pressure sensor due to the jitter of fingers while grasping, as well as the magnetic hysteresis of the MR brake [53]. Consequently, a more superior control scheme is still required by comprehensively considering the time delay and hysteresis effect. In addition, a more accurate method for the feedback force measurement that are not affected by the finger jitter is needed in future works.

V. CONCLUSION

This study is concerned with the development and feedback force control of a safe, lightweight, powerful, and stable MR brake-based passive FFDG. First, the mechanical design of the FFDG is presented. In the design, a small-scale disc-type MR brake is utilized as the force feedback device, and the generated feedback force is transmitted to the operator's fingertips though a flexible Bowden-cable transmission mechanism. Also, an indirect-type angle measuring mechanism is designed to detect the finger joint angle. Subsequently, a buck circuit-based current controller is designed and modelled combining with the control mode of the MR brake. Thereafter, the feedback force tracking control is conducted using conventional PID and adaptive fuzzy-PID control schemes. Through simulations, the control effect of the two methods is evaluated, and the results indicate that the adaptive fuzzy-PID controller is more favorable for the feedback force control. Several tests are conducted to evaluate the force output and response characteristics of the MR brake. It is found that the effect of rotational speed is minimal on the resistance force and the friction force is negligible compared with the field-induced force. The time lag of current controller accounts for the majority of the total response time through force response experiments. By contrast, the response time of the MR brake is extremely very small, only about 10 ms at 1 A. Finally, an experimental set-up is established, and several experiments are carried out on the FFDG prototype. The designed angle measuring mechanism is proved to be feasible and accurate through angle measuring experiments. Moreover, the feedback force generated by the MR brake exhibits steadily during the entire grasping process, and it is less affected by the grasping speed. Furthermore, the results of the feedback force tracking control experiments, in cases of both ramp and sinusoidal signals, demonstrate that the

feedback force tracking accuracy of the adaptive fuzzy-PID controller is satisfactory.

REFERENCES

[1] R. Miyazaki, K. Hirose, Y. Ishikawa, T. Kanno, and K. Kawashima, "A master–slave integrated surgical robot with active motion transformation using wrist axis," *IEEE/ASME Trans. Mechatronics*, vol. 23, no. 3, pp. 1215–1225, Jun. 2018.

[2] Y. Lin, H. Zhao, Y. Zhang, and H. Ding, "A data-driven motion mapping method for space teleoperation of kinematically dissimilar master/slave robots," in *Proc. IEEE Int. Conf. Robot. Biomim.*, Dec. 2018, pp. 862–867.

[3] X. Xu, A. Song, D. Ni, H. Li, P. Xiong, and C. Zhu, "Visual-haptic aid teleoperation based on 3-D environment modeling and updating," *IEEE Trans. Ind. Electron.*, vol. 63, no. 10, pp. 6419–6428, Oct. 2016.

[4] W. Li, N. Yang, J. Wang, and D. Ren, "Kinematic teleoperation of wheeled mobile robot with slippage compensation on soft terrains," *IEEE Access*, vol. 7, pp. 110982–110991, 2019.

[5] J. Blake and H. B. Gurocak, "Haptic glove with MR brakes for virtual reality," *IEEE/ASME Trans. Mechatronics*, vol. 14, no. 5, pp. 606–615, Oct. 2009.

[6] I. Dimbwadyo-Terrer, F. Trincado-Alonso, A. de los Reyes-Guzmán, M. A. Aznar, C. Alcubilla, S. Pérez-Nombela, A. del Ama-Espinosa, B. Polonio-López, and Á. Gil-Agudo, "Upper limb rehabilitation after spinal cord injury: A treatment based on a data glove and an immersive virtual reality environment," *Disabil. Rehabil. Assist. Technol.*, vol. 11, no. 6, pp. 462–467, Jul. 2016.

[7] X. Gu, Y. Zhang, W. Sun, Y. Bian, D. Zhou, and P. O. Kristensson, "Dexmo: An inexpensive and lightweight mechanical exoskeleton for motion capture and force feedback in VR," in *Proc. CHI Conf. Hum. Factors Comput. Syst.*, May 2016, pp. 1991–1995.

[8] J. S. Ruth and K. Dhanalakshmi, "Shape memory alloy with bi-functionality in the master system to control a slave," *Sens. Actuators A, Phys.*, vol. 238, pp. 351–360, Feb. 2016.

[9] M. Bouzit, G. Burdea, G. Popescu, and R. Boian, "The Rutgers Master II-new design force-feedback glove," *IEEE/ASME Trans. Mechatronics*, vol. 17, no. 2, pp. 256–263, Jun. 2002.

[10] S. Nakagawara, H. Kajimoto, N. Kawakami, S. Tachi, and I. Kawabuchi, "An encounter-type multi-fingered master hand using circuitous joints," in *Proc. IEEE Int. Conf. Robot. Autom.*, Apr. 2005, pp. 2667–2672.

[11] P. Ben-Tzvi and Z. Ma, "Sensing and force-feedback exoskeleton (SAFE) robotic glove," *IEEE Trans. Neural Syst. Rehabil. Eng.*, vol. 23, no. 6, pp. 992–1002, Nov. 2015.

[12] P. Ben-Tzvi, J. Danoff, and Z. Ma, "The design evolution of a sensing and force-feedback exoskeleton robotic glove for hand rehabilitation application," *J. Mech. Robot.*, vol. 8, no. 5, Oct. 2016, Art. no. 051019.

[13] Z. Ma, P. Ben-Tzvi, and J. Danoff, "Hand rehabilitation learning system with an exoskeleton robotic glove," *IEEE Trans. Neural Syst. Rehabil. Eng.*, vol. 24, no. 12, pp. 1323–1332, Dec. 2016.

[14] D. Hwang, J. Lee, and K. Kim, "On the design of a miniature haptic ring for cutaneous force feedback using shape memory alloy actuators," *Smart Mater. Struct.*, vol. 26, no. 10, Sep. 2017, Art. no. 105002.

[15] N. A. Mansour, A. M. F. El-Bab, S. F. Assal, and O. Tabata, "Design, characterization and control of SMA springs-based multi-modal tactile display device for biomedical applications," *Mechatronics*, vol. 31, pp. 255–263, 2015.

[16] M. I. Tiwana, S. J. Redmond, and N. H. Lovell, "A review of tactile sensing technologies with applications in biomedical engineering," *Sens. Actuators A, Phys.*, vol. 179, pp. 17–31, Jun. 2012.

[17] P. Olsson, F. Nysjö, I. B. Carlbom, and S. Johansson, "Comparison of walking and traveling-wave piezoelectric motors as actuators in kinesthetic haptic devices," *IEEE Trans. Haptics*, vol. 9, no. 3, pp. 427–431, Jul./Sep. 2016.

[18] B. Sauvet, T. Laliberte, and C. Gosselin, "Design, analysis and experimental validation of an ungrounded haptic interface using a piezoelectric actuator," *Mechatronics*, vol. 45, pp. 100–109, Aug. 2017.

[19] A. Mazursky, J.-H. Koo, and T.-H. Yang, "Design, modeling, and evaluation of a slim haptic actuator based on electrorheological fluid," *J. Intell. Mater. Syst. Struct.*, vol. 30, no. 17, pp. 2521–2533, 2019.

[20] Y. M. Han, J. S. Oh, S. Kim, and S. B. Choi, "Design of multi-degree motion haptic mechanisms using smart fluid-based devices," *Mech. Based Des. Struct. Mech.*, vol. 45, no. 1, pp. 135–144, 2017.

[21] Y. H. Hwang, S. R. Kang, S. W. Cha, and S. B. Choi, "A robot-assisted cutting surgery of human-like tissues using a haptic master operated by magnetorheological clutches and brakes," *Smart Mater. Struct.*, vol. 28, no. 6, May 2019, Art. no. 065016.

[22] D. Chen, A. Song, X. Hu, L. Fu, and Q. Ouyang, "A spherical actuator-based hand-held haptic device for touch screen interaction," *IEEE Access*, vol. 7, pp. 15125–15139, 2019.

[23] H. Qin, A. Song, and Y. Mo, "Evaluation of a multi-drum magnetorheological brake via finite element analysis considering number of drums and fluid gap selection in optimization," *J. Intell. Mater. Syst. Struct.*, vol. 30, no. 5, pp. 778–787, 2019.

[24] D. Wang, B. Zi, S. Qian, and J. Qian, "Steady-state heat-flow coupling field of a high-power magnetorheological fluid clutch utilizing liquid cooling," *J. Fluids Eng.-Trans. ASME*, vol. 139, no. 11, Nov. 2017, Art. no. 111105.

[25] S. H. Winter and M. Bouzit, "Use of Magnetorheological Fluid in a Force Feedback Glove," *IEEE Trans. Neural Syst. Rehabil. Eng.*, vol. 15, no. 1, pp. 2–8, Mar. 2007.

[26] D. Chen, A. Song, L. Tian, H. Zeng, and P. Xiong, "Development of a multidirectional controlled small-scale spherical MR actuator for haptic applications," *IEEE/ASME Trans. Mechatronics*, vol. 24, no. 4, pp. 1597–1607, Aug. 2019, doi: 10.1109/TMECH.2019.2916099.

[27] D. J. Cassar and M. A. Saliba, "A force feedback glove based on magnetorheological fluid: Preliminary design issues," in *Proc. 15th IEEE Mediterr. Electrotech. Conf.*, Apr. 2010, pp. 618–623.

[28] H. Qin, A. Song, Z. Gao, Y. Liu, and G. Jiang, "A multi-finger interface with mr actuators for haptic applications," *IEEE Trans. Haptics*, vol. 11, no. 1, pp. 5–14, Jan./Mar. 2018.

[29] M. Okui, M. Kobayashi, Y. Yamada, and D. Nakamura, "Delta-type four-DOF force-feedback device composed of pneumatic artificial muscles and magnetorheological clutch and its application to lid opening," *Smart Mater. Struct.*, vol. 28, no. 6, May 2019, Art. no. 064003.

[30] M. W. Uddin, X. Zhang, and D. Wang, "A pneumatic-driven haptic glove with force and tactile feedback," in *Proc. Int. Conf. Virtual Reality Vis. (ICVRV)*, Sep. 2016, pp. 304–311.

[31] A. Wege and G. Hommel, "Development and control of a hand exoskeleton for rehabilitation of hand injuries," in *Proc. IEEE/RSJ Int. Conf. Intell. Robot. Syst.*, Aug. 2005, pp. 3046–3051.

[32] H. Fang, Z. Xie, H. Liu, T. Lan, and J. Xia, "An exoskeleton force feedback master finger distinguishing contact and non-contact mode," in *Proc. IEEE/RSJ Int. Conf. Intell. Robot. Syst.*, Jul. 2009, pp. 1059–1064.

[33] H. Fang, Z. Xie, and H. Liu, "An exoskeleton master hand for controlling DLR/HIT hand," in *Proc. IEEE/RSJ Int. Conf. Intell. Robot. Syst.*, Oct. 2009, pp. 3703–3708.

[34] S. Das, Y. Kishishita, T. Tsuji, C. Lowell, K. Ogawa, and Y. Kurita, "ForceHand glove: A wearable force-feedback glove with pneumatic artificial muscles (PAMs)," *IEEE Robot. Autom. Lett.*, vol. 23, no. 3, pp. 2416–2423, Jul. 2018.

[35] H. Ma, B. Chen, L. Qin, and W. H. Liao, "Design and testing of a regenerative magnetorheological actuator for assistive knee braces," *Smart Mater. Struct.*, vol. 26, no. 3, Feb. 2017, Art. no. 035013.

[36] J. W. Sohn, J. Jeon, Q. H. Nguyen, and S. B. Choi, "Optimal design of disc-type magneto-rheological brake for mid-sized motorcycle: Experimental evaluation," *Smart Mater. Struct.*, vol. 24, no. 8, Jul. 2015, Art. no. 085009.

[37] W. Li, H. Du, H. Zhang, D. Ning, S. Sun, W. Li, and Y. Wang, "Design and testing of a novel two-way controllable overrunning clutch based magnetorheological brake," *Smart Mater. Struct.*, vol. 28, no. 9, Aug. 2019, Art. no. 095013.

[38] X. Yin, S. Guo, N. Xiao, T. Tamiya, H. Hirata, and H. Ishihara, "Safety operation consciousness realization of a MR fluids-based novel haptic interface for teleoperated catheter minimally invasive neurosurgery," *IEEE/ASME Trans. Mechatronics*, vol. 21, no. 2, pp. 1043–1054, Apr. 2016.

[39] X. Yin, S. Guo, H. Hirata, and H. Ishihara, "Design and experimental evaluation of a teleoperated haptic robot–assisted catheter operating system," *J. Intell. Mater. Syst. Struct.*, vol. 27, no. 1, pp. 3–16, Nov. 2016.

[40] Y. Song, S. Guo, X. Yin, L. Zhang, Y. Wang, H. Hirata, and H. Ishihara, "Design and performance evaluation of a haptic interface based on MR fluids for endovascular tele-surgery," *Microsyst. Technol.*, vol. 24, no. 2, pp. 909–918, Feb. 2018.

[41] A. Chiri, N. Vitiello, F. Giovacchini, S. Roccella, F. Vecchi, and M. C. Carrozza, "Mechatronic Design and Characterization of the Index Finger Module of a Hand Exoskeleton for Post-Stroke Rehabilitation," *IEEE/ASME Trans. Mechatronics*, vol. 17, no. 5, pp. 884–894, Oct. 2012.

[42] C. Rossa, L. Eck, A. Micaelli, and J. Lozada, "On a novel torque detection technique for magnetorheological actuators," *IEEE Sensors J.*, vol. 14, no. 4, pp. 1223–1231, Apr. 2013.
[43] H. Qin, A. Song, and Y. Mo, "Performance evaluation of a hollowed multi-drum magnetorheological brake based on finite element analysis considering hollow casing radius," *IEEE Access*, vol. 7, pp. 96070–96078, 2019.
[44] D. Wang, Z. Tian, Q. Meng, and Y. Hou, "Development of a novel two-layer multiplate magnetorheological clutch for high-power applications," *Smart Mater. Struct.*, vol. 22, no. 8, Jul. 2013, Art. no. 085018.
[45] T. Türker, U. Buyukkeles, and A. F. Bakan, "A robust predictive current controller for PMSM drives," *IEEE Trans. Ind. Electron.*, vol. 63, no. 6, pp. 3906–3914, Jun. 2016.
[46] F. Peng, J. Ye, and A. Emadi, "A digital PWM current controller for switched reluctance motor drives," *IEEE Trans. Power Electron.*, vol. 31, no. 10, pp. 7087–7098, Oct. 2016.
[47] H. Li-yong, Z. Xi-lin, Z. Di, and Z. Jian-Ming, "Numerical simulation of fuzzy-PID tension control system based on rotary MRF damper," in *Proc. Int. Conf. Intell. Hum.-Mach. Syst. Cybern.*, Aug. 2009, pp. 133–137.
[48] A. A. Zamani, S. Tavakoli, S. Etedali, and J. Sadeghi, "Adaptive fractional order fuzzy proportional–integral–derivative control of smart base-isolated structures equipped with magnetorheological dampers," *J. Intell. Mater. Syst. Struct.*, vol. 29, no. 5, pp. 830–844, Aug. 2018.
[49] K. Eltag, M. S. Aslamx, and R. Ullah, "Dynamic stability enhancement using fuzzy PID control technology for power system," *Int. J. Control Autom. Syst.*, vol. 17, no. 1, pp. 234–242, Jan. 2019.
[50] S. Etedali and S. Tavakoli, "PD/PID controller design for seismic control of high-rise buildings using multi-objective optimization: A comparative study with LQR controller," *J. Earthq. Tsunami* , vol. 11, no. 3, Sep. 2017, Art. no. 1750009.
[51] A. A. Zamani, S. Tavakoli, and S. Etedali, "Control of piezoelectric friction dampers in smart base-isolated structures using self-tuning and adaptive fuzzy proportional–derivative controllers," *J. Intell. Mater. Syst. Struct.*, vol. 28, no. 10, pp. 1287–1302, Sep. 2017.
[52] T. Abut and S. Soyguder, "Real-time control and application with self-tuning PID-type fuzzy adaptive controller of an inverted pendulum," *Ind. Robot.*, vol. 46, no. 1, pp. 159–170, Jan. 2019.
[53] H. Qin, A. Song, and Y. Mo, "A hybrid actuator with hollowed multi-drum magnetorheological brake and direct-current micromotor for hysteresis compensation," *J. Intell. Mater. Syst. Struct.*, vol. 30, no. 7, pp. 1031–1042, 2019.

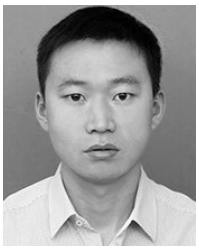

DAOMING WANG received the Ph.D. degree in mechanical engineering from the China University of Mining and Technology, in 2014. He is currently an Associate Professor with the School of Mechanical Engineering, Hefei University of Technology. His research interests mainly include robotics, mechatronic, and smart materials. His research has led to publications of over 30 technical articles in international journals and conference proceedings.

YAKUN WANG is currently pursuing the master's degree with the School of Mechanical Engineering, Hefei University of Technology, China. His research interests include rehabilitation robotics and mechatronics.

JIAWEI PANG received the master's degree in mechanical engineering from the Hefei University of Technology, in 2019. His research interests include force feedback date glove and smart materials.

ZHENGYU WANG received the Ph.D. degree in mechanical engineering from Harbin Engineering University, Harbin, China, in 2017. He is currently a Lecturer with the School of Mechanical Engineering, Hefei University of Technology, Hefei, China. He has authored or coauthored more than 20 journal and conference publications. His research interests include mechatronics, haptic interaction, and surgical robotics.

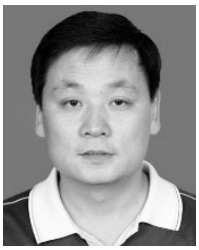

BIN ZI received the Ph.D. degree in mechatronic engineering from Xidian University, Xi'an, China, in 2007. He was a Visiting Scholar with the Chair of Mechanics and Robotics, University of Duisburg-Essen, Germany, from 2011 to 2012. He was a Visiting Professor with the Robotics and Automation Laboratory, Institute of Technology, University of Ontario, Canada, in 2015. He is currently a Professor and the Dean of School of Mechanical Engineering, Hefei University of Technology, Hefei, China. He has authored or coauthored two monographs and more than 100 journal and conference publications. His research interests include robotics and automation, mechatronics, and multirobot systems.